Imperial College London

4M Finite Element Analysis and Applications M-Level Project

Imperial College London

Department of Mechanical Engineering

Petro-Chemical Pressure Vessel Stress Analysis

Author:

Fiona Boyce

Lecturer:

Dr Ulrich Hansen

Word Count:

1237

April 28, 2019

Contents

List of Figures

List of Tables

1 Introduction

The client has requested a stress analysis investigation into a medium carbon steel petrochemical pressure vessel. Figure 1 shows a diagram of the pressure to be analysed with a blown up view of the section of interest. The vessel experiences a pressure increase of 15 atm during operation and is supported with rolling supports at its mid-section. An expansion bellows unit attaches the nozzle to the pipework, so that the forces on the end of the nozzle are negligible. The significance of this with respect to finite element modelling is discussed further in Section 2.2.

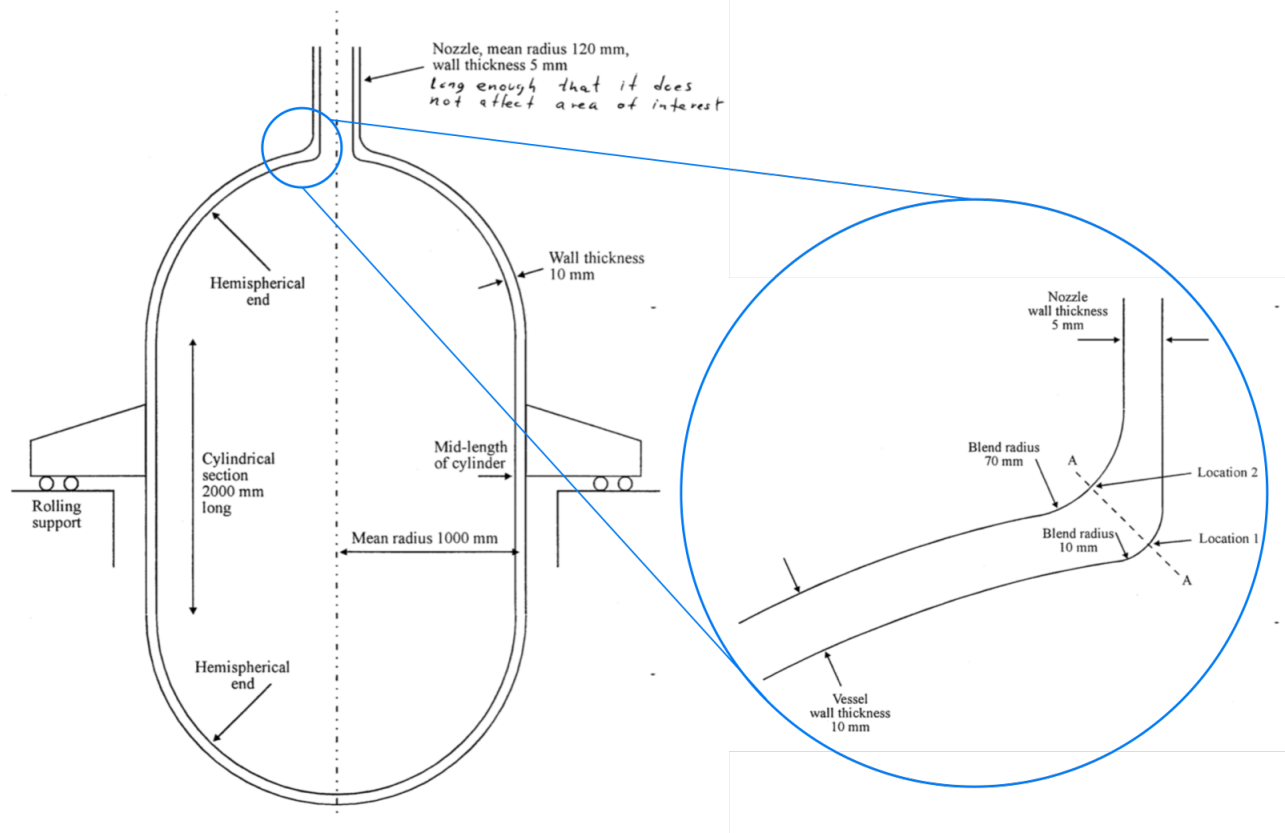

Figure 1: Diagram of the pressure vessel and section of interest

2 Finite Element Models

The pressure vessel is axisymmetric so the model was created as an infinitely thin 2D slice with 8 noded quadratic elements and axisymmetric behavior. Initial meshes contained only structured quadrilateral elements, however during the optimisation process a mesh with a section of unstructured triangular quadratic elements was included as well, to create a transition between a fine and coarse mesh, allowing the number of elements width wise across the model to change.

2.1 Loads and Boundary Conditions

Figure 2 shows the geometry of the pressure vessel that was modelled. The load is shown in blue, representing the internal pressure increase of 15 atmospheres. The only boundary condition was restraining the nodes along the bottom line (marked in green on the diagram) in the y direction. For clarity, the global coordinate system is shown in orange. The weight of the pressure vessel was considered negligible.

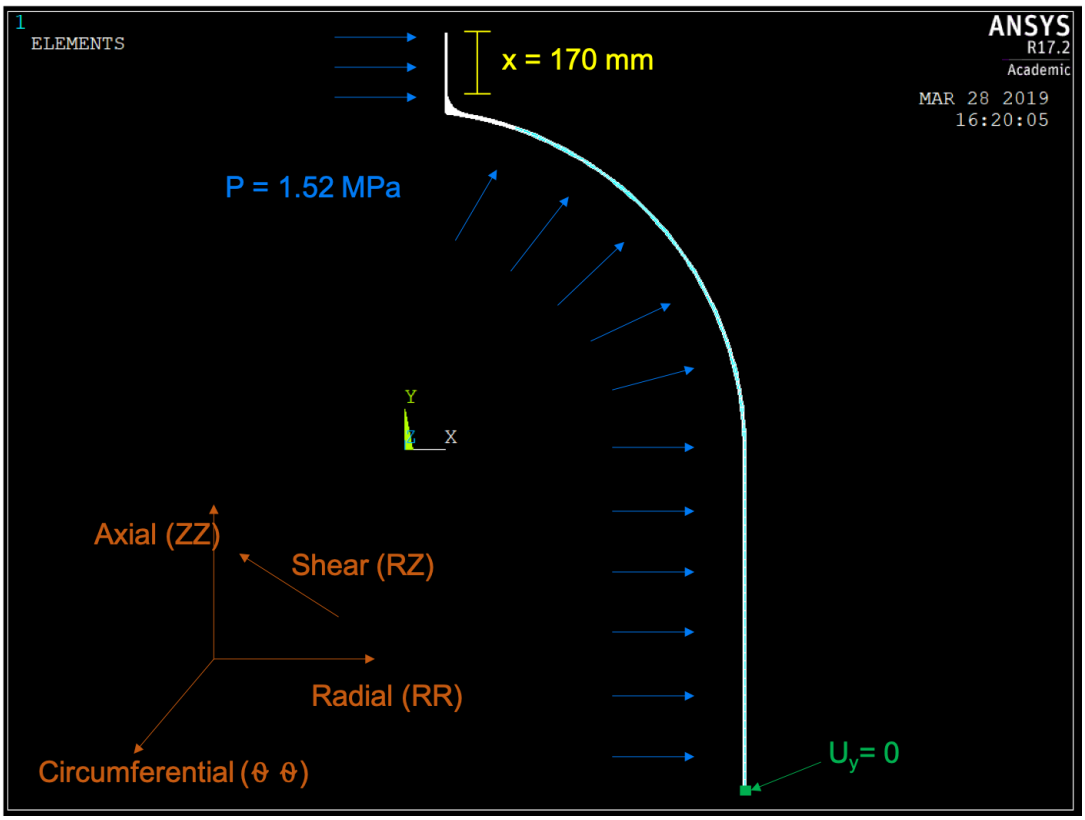

Figure 2: Loads and Boundary Conditions

Modelling the entire pressure vessel geometry (even as a 2D slice) is a waste of computational time. The cylindrical portion of the pressure vessel expands twice as much as the

hemispherical sections, this behavior is demonstrated in Figure 3, and was modelled in order to check that the behavior was as expected. The transitional stress region marked shows the point in the geometry where the vessel becomes cylindrical. It is important to note that this diagram is not to scale, it's exaggerated in order to show where the deformation would occur. The FE model was cut off at the roller joints as the radial expansion is not inhibited so the reaction force is 0. Therefore all boundary conditions for this portion of the pressure vessel are known and it can be modelled efficiently and accurately.

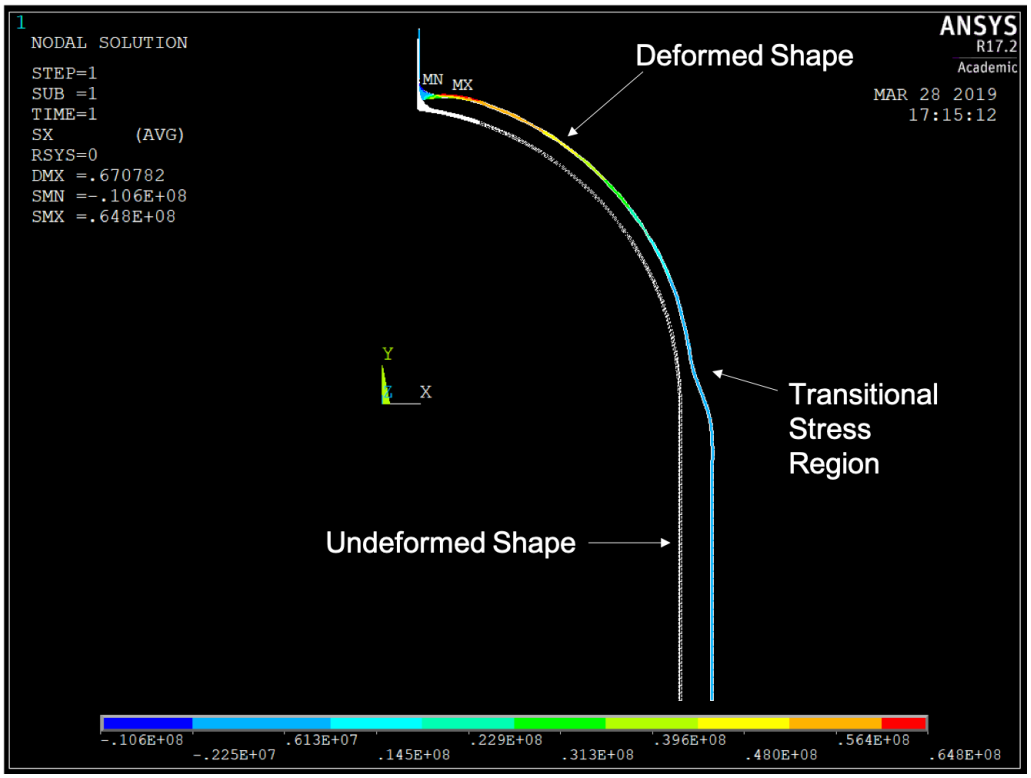

Figure 3: Deformed and un-deformed models of the pressure vessel.

2.2 Nozzle Length

The pressure vessel nozzle is fitted with expansion bellows so that no significant forces are felt at the end of the nozzle. In order to model this accurately, the length of the nozzle needed to be long enough so that the stresses were negligible at the nozzle end, but not so long that it was unnecessary. To get an accurate value for this, a graph of the decay of the stress components in a pipe was generated specifically for this pressure vessel, adapted from the functions given in [1] as shown in Figure 4. The stresses appear to become negligible at about 0.12m, however upon closer inspection stresses were still found to be present until about 0.17m, hence 0.17m was selected as shown in Figure 2.

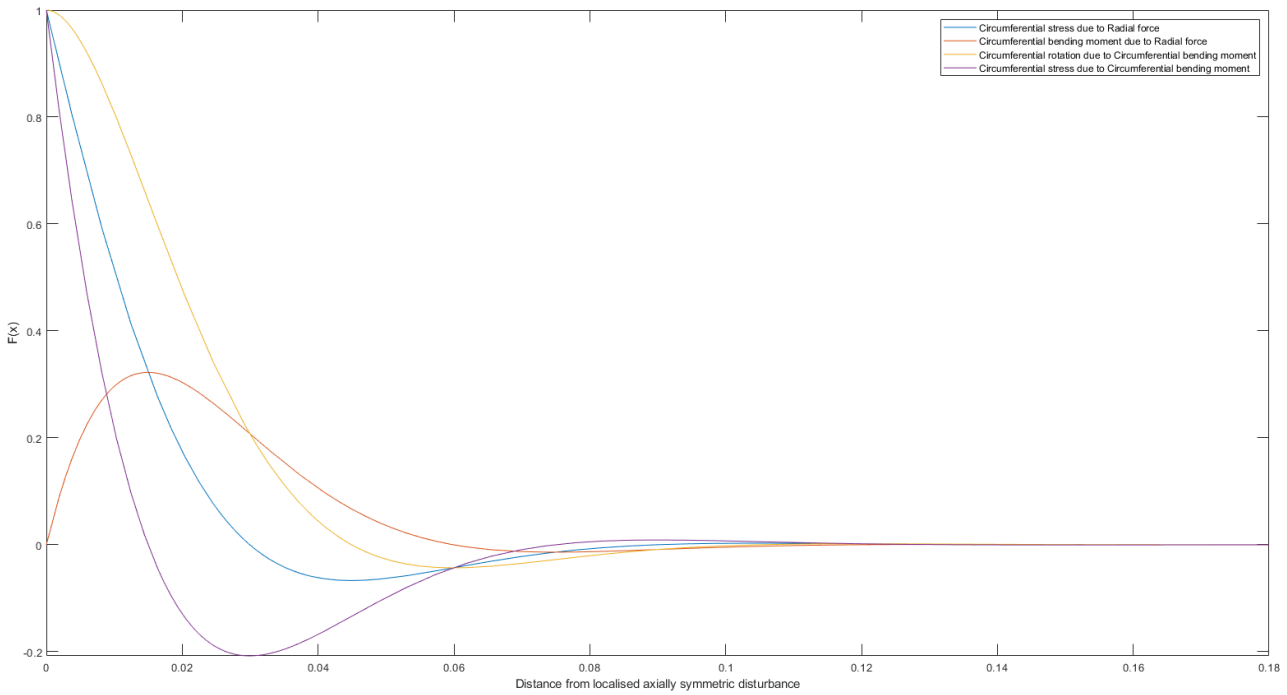

Figure 4: Stress decay in the pressure vessel nozzle

2.3 Mesh Optimisation

To get the balance between a fine mesh for accurate results, but without being fine across the entire model (wasting computing time) the model was split into different sections with a mostly structured mesh. Size controls were implemented to ensure the width-wise number of elements stayed the same across the areas. In the area of interest (See Figure 1) the mesh was kept extremely fine to get the most accurate results, 16 elements across. however to prevent requiring a fine mesh throughout the model, an area was set to be unstructured with quadratic triangular elements as shown in Figure 5, reducing the total number of elements required to complete the model.

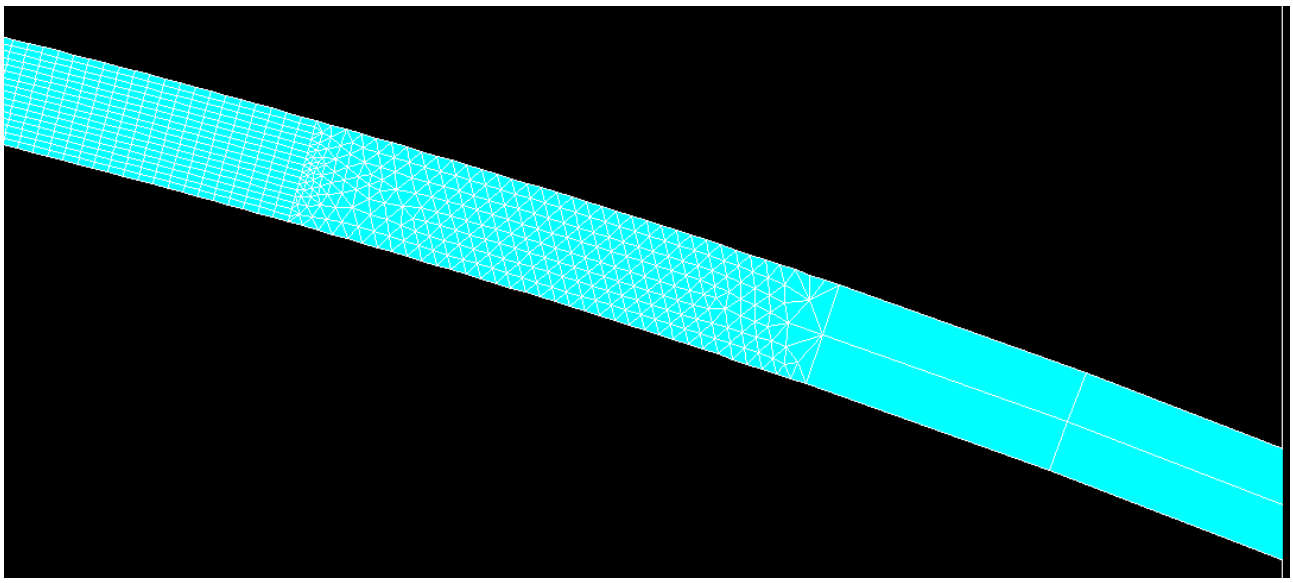

Figure 5: Unstructured area of the model

3 Convergence

The results of the convergence study are shown in Figures 6, 7, 8 and 9. The study involved taking the areas of the mesh with structured grids and increasing the number of elements normal to the geometry. 6 across was used as an initial estimate, and the most fine mesh was used at 16 elements wide. When changing the element sizing on the structured portions of the mesh, the sizing of the elements in the tangential direction needed to be changed too, this was to prevent any elements being too elongated in the mesh (avoiding long thin elements with aspect ratios larger than 3 and angular distortions less than 30 degrees). To give more control over this, the model was split into 5 sections, and each part had a different size control in the direction tangential to the geometry of the model. This was done to ensure each section had elements that were as square as possible, and blended smoothly into each area, without big differences in size between elements.

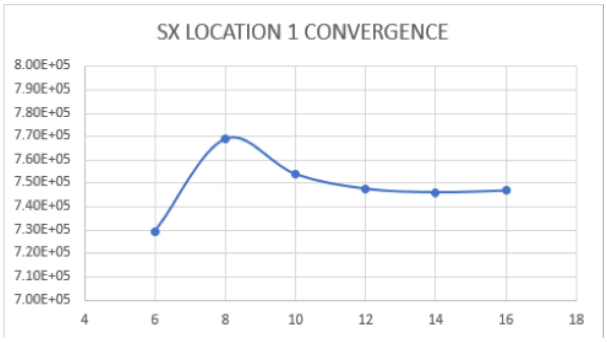

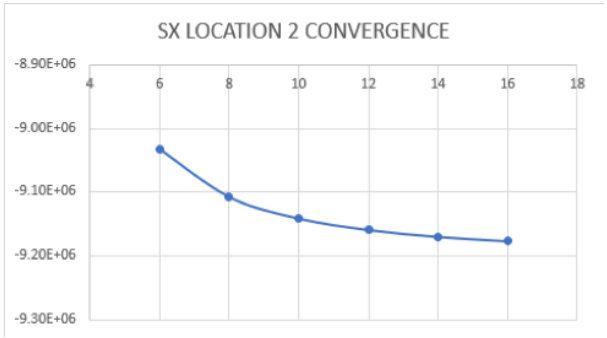

Figure 6: Radial Stress Convergence

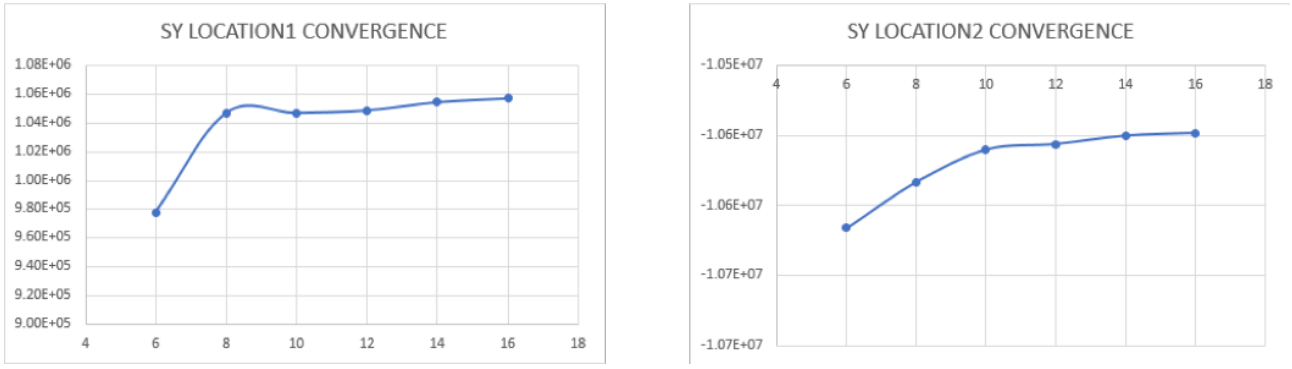

Figure 7: Axial Stress Convergence

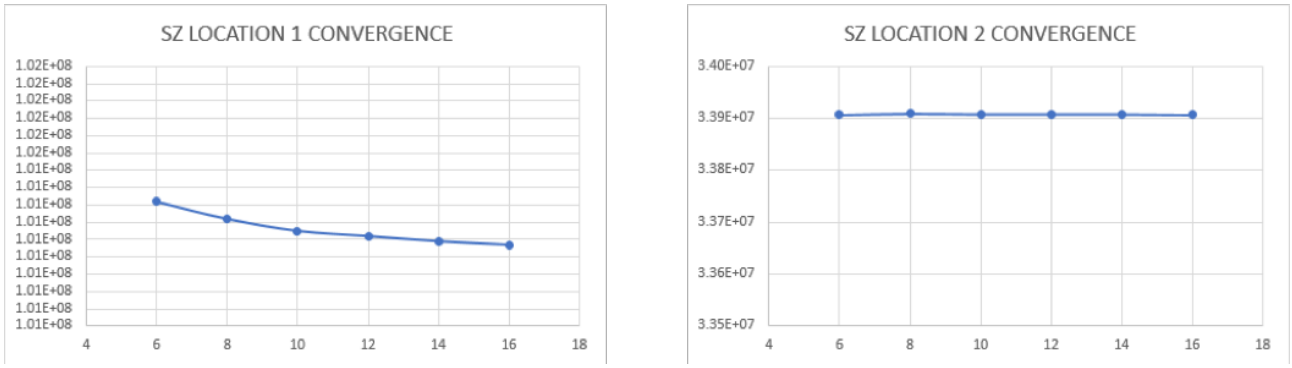

Figure 8: Circumferential Stress Convergence

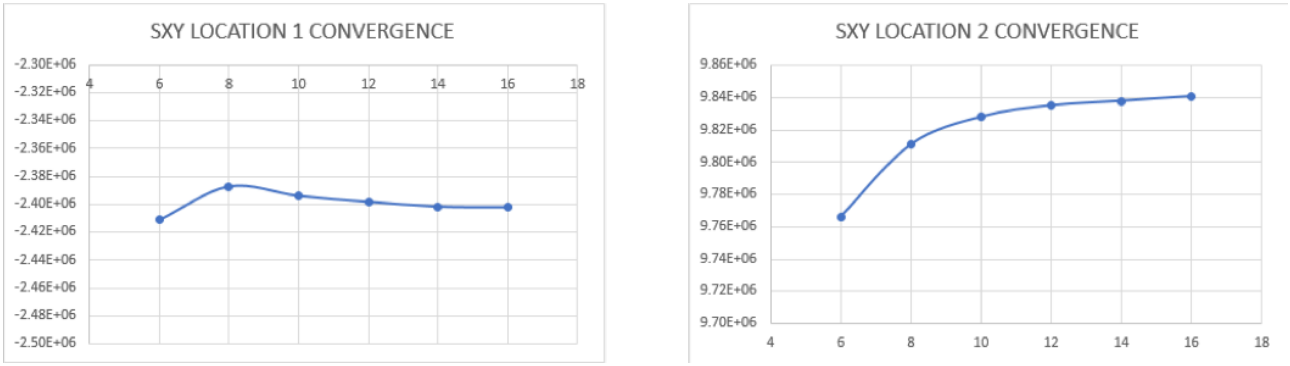

Figure 9: Shear Stress Convergence

4 Verification

In order to ensure the finite element model was accurate, the stresses at various nodes calculated with finite element analysis were compared against numbers calculated analytically. Figure 10 shows the rough locations of each of the nodes. Node 11657 was used to calculate the stresses at the nozzle, 40 for the hemisphere and 7485 for the cylinder. These are shown in Table 1. It should be noted that the errors for the FE values are too high for the stresses in the hemispherical section, this is because of the geometry of the model. The transitional area

(shown in Figure 3) combined with the global coordinate system meant that the hemispherical solutions were off. In order to fully verify the model, the principal stresses were used instead as they were accurate regardless of the coordinate system. A reason the values are not perfect could lie in the assumptions for the calculations. The nozzle was modelled as an open ended cylinder while the hemispherical and cylindrical sections of the pressure vessel were modelled as close ended.

Nozzle Stresses (Pa)						
	Analytical	FE @ 11657	FE Error	Principal Stresses		PS Error
Hoop(SZ)	3.65E+07	3.65E+07	0.08%	S1	3.65E+07	0.08%
Radial (SX)	-1.52E+06	-1.52E+06	0.01%	S2	-1519900	0.01%
Axial (SY)	1.82E+07	5.40E+04	99.70%	S3	5.40E+04	99.70%
Hemisphere Stresses (Pa)						
	Analytical	FE @40	FE Error	Principal Stresses		PS Error
Hoop(SZ)	7.60E+07	8.52E+07	12.09%	S1	7.77E+07	-2.19%
Radial (SX)	-1.52E+06	-5.92E+05	-61.04%	S2	-1.53E+06	-0.42%
Axial (SY)	7.60E+07	9.20E+07	21.00%	S3	7.36E+07	3.18%
Cylinder Stresses (Pa)						
	Analytical	FE @7485	FE Error	Principal Stresses		PS Error
Hoop(SZ)	1.52E+08	1.52E+08	0.01%	S1	1.52E+08	0.01%
Radial (SX)	-1.52E+06	-1.52E+06	0.06%	S2	-1.52E+06	0.06%
Axial (SY)	7.60E+07	7.42E+07	2.43%	S3	7.42E+07	2.43%

Table 1: Analytic solutions vs FE results

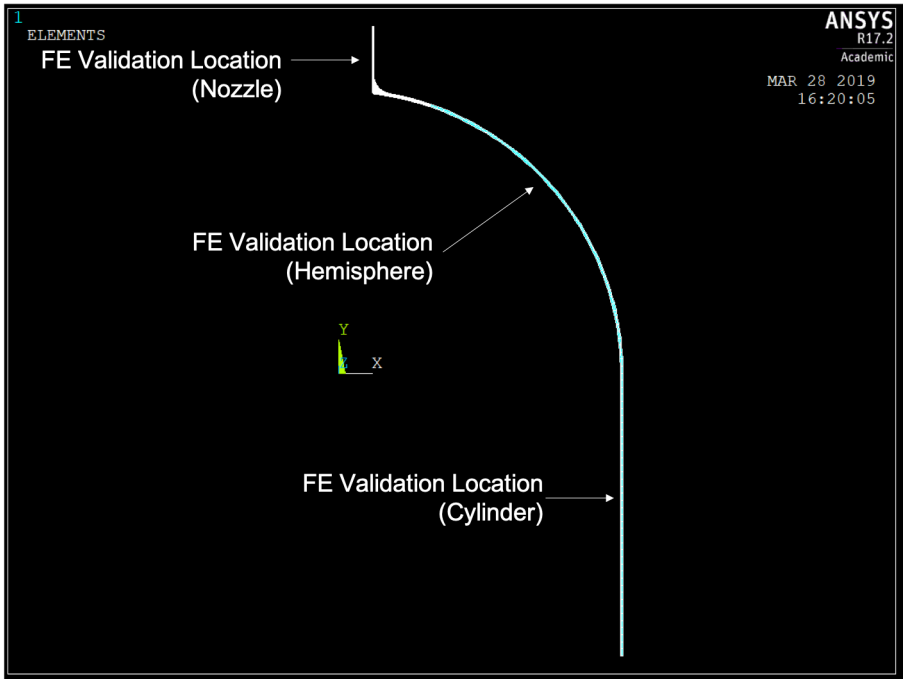

Figure 10: Validation node locations

5 Results and Discussion

The stress distributions across the wall thickness at the section marked AA are found in Figure 11. Tabulated values of the stresses at locations 1 and 2 are found in Table 2.

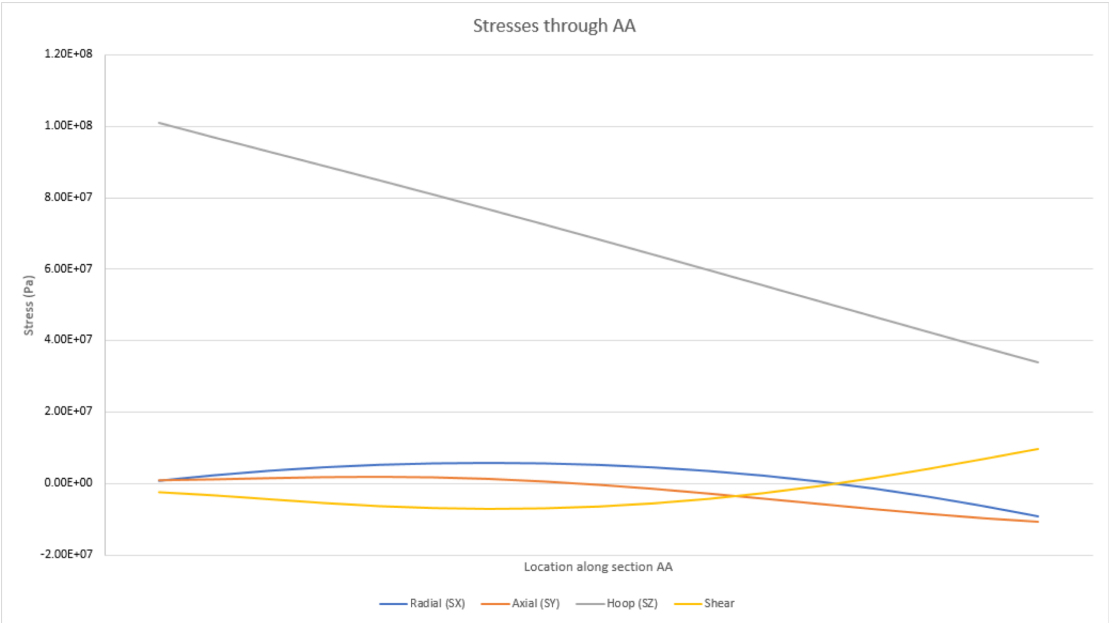

Figure 11: Stresses through Section AA

The contour plots of the stresses in the vicinity of the intersection are found in Figures 12, 13, 14 and 15. It should be noted however that these stresses are calculated in accordance

Type	Stress at Location 1 (MPa)	Stress at Location 2 (MPa)
Radial	0.747	-9.18
Axial	1.06	-10.50
Circumferential	101.00	33.90
Shear	-2.40	9.84

Table 2: Stress Values at Locations 1 and 2

with the global coordinate system, the local coordinate system will change between the hemispherical and cylindrical portions of the pressure vessel. To account for this, principal stress contour plots are also provided (in Figures 16, 17 and 18) representing the maximum normal stress calculated when the shear stress is zero.

A Von-Mises contour plot is shown in Figure 19 which shows the stresses independent of the coordinate system for comparison.

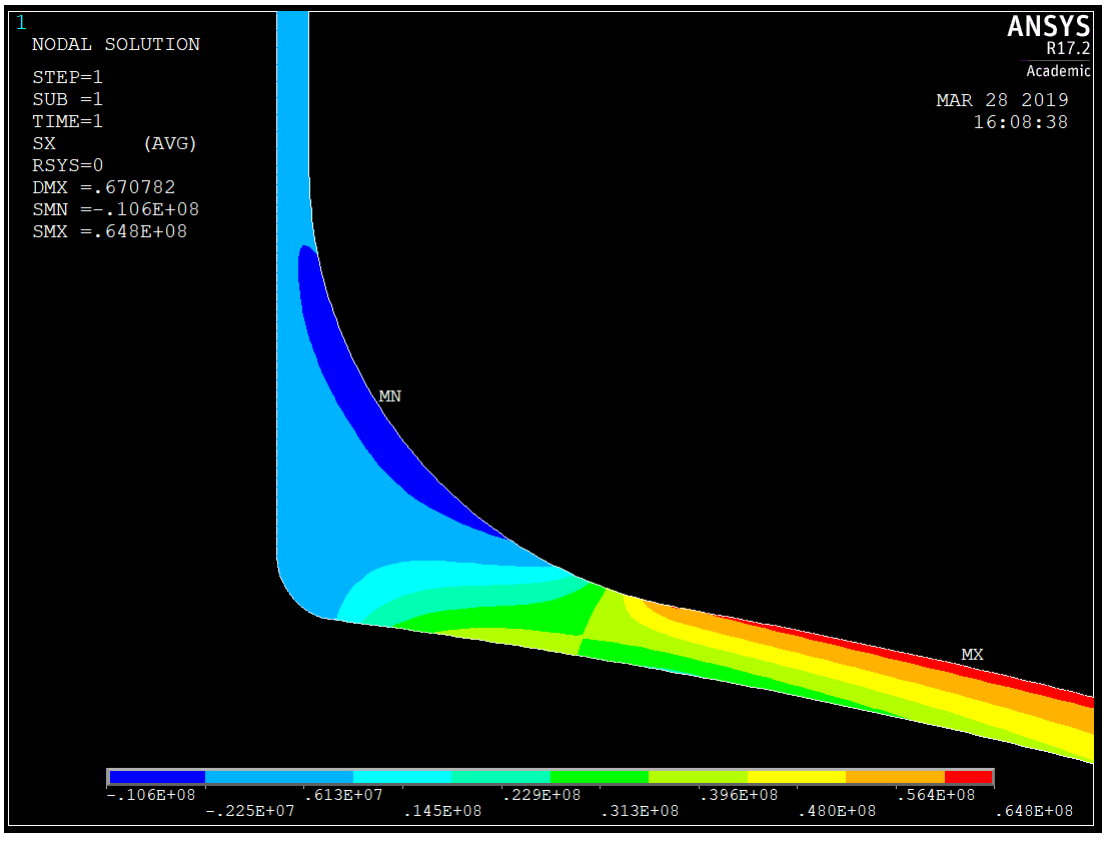

Figure 12: Radial Stress (RR) Contour Plot

As seen in the diagrams, the shear stress is greatest at the outer surface of the fillet between the nozzle and pressure vessel, while the von mises and circumferential stresses are greatest at the inner surface of the join between the nozzle and pressure vessel.

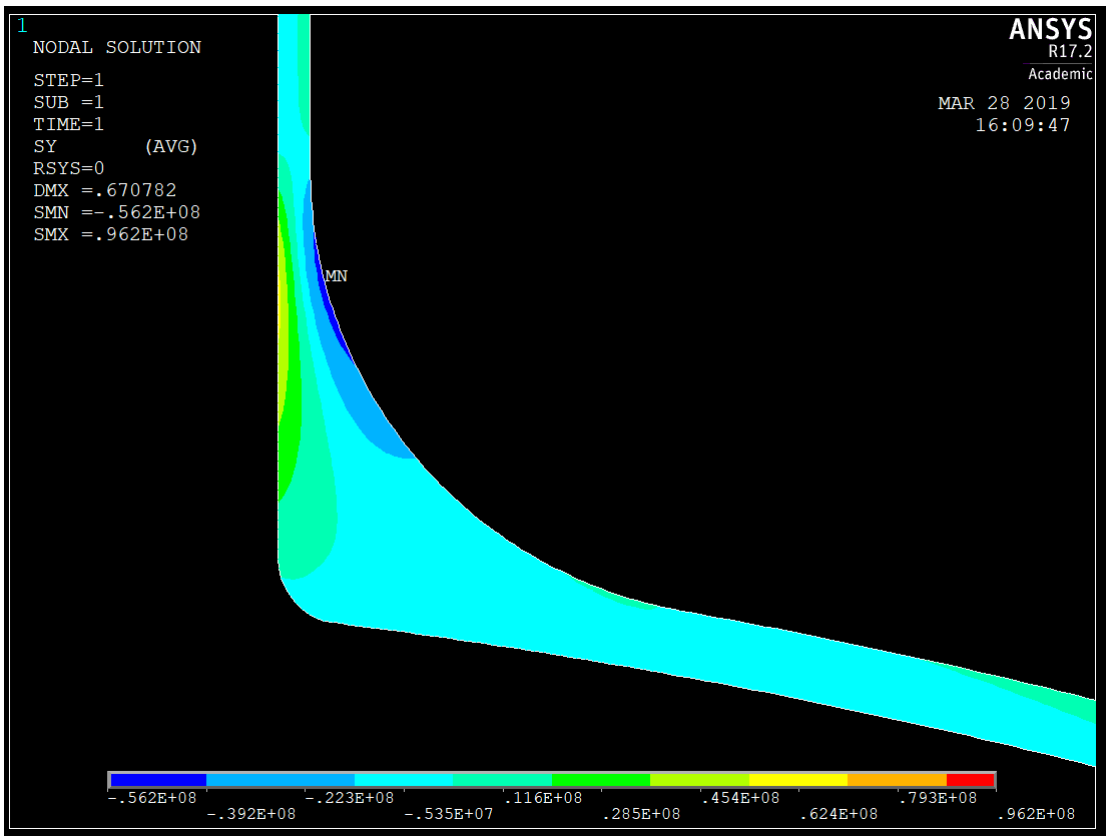

Figure 13: Axial Stress (ZZ) Contour Plot

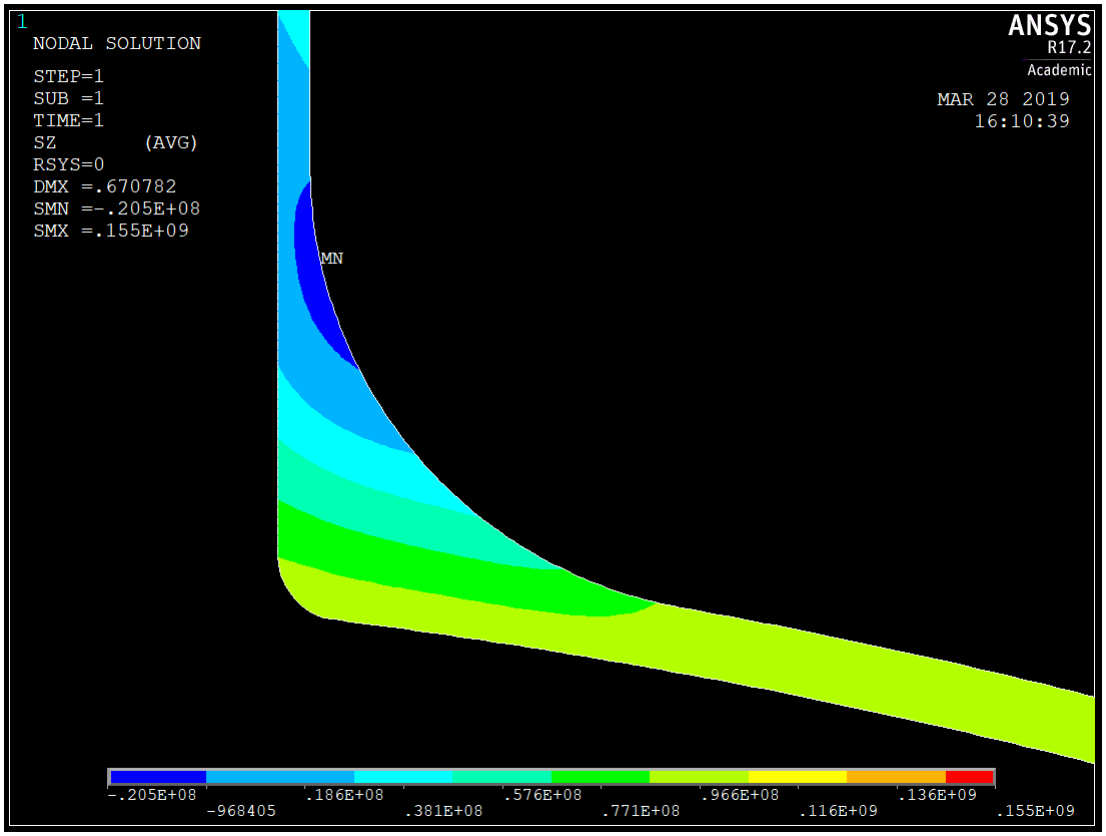

Figure 14: Circumferential Stress ($\theta\theta$) Contour Plot

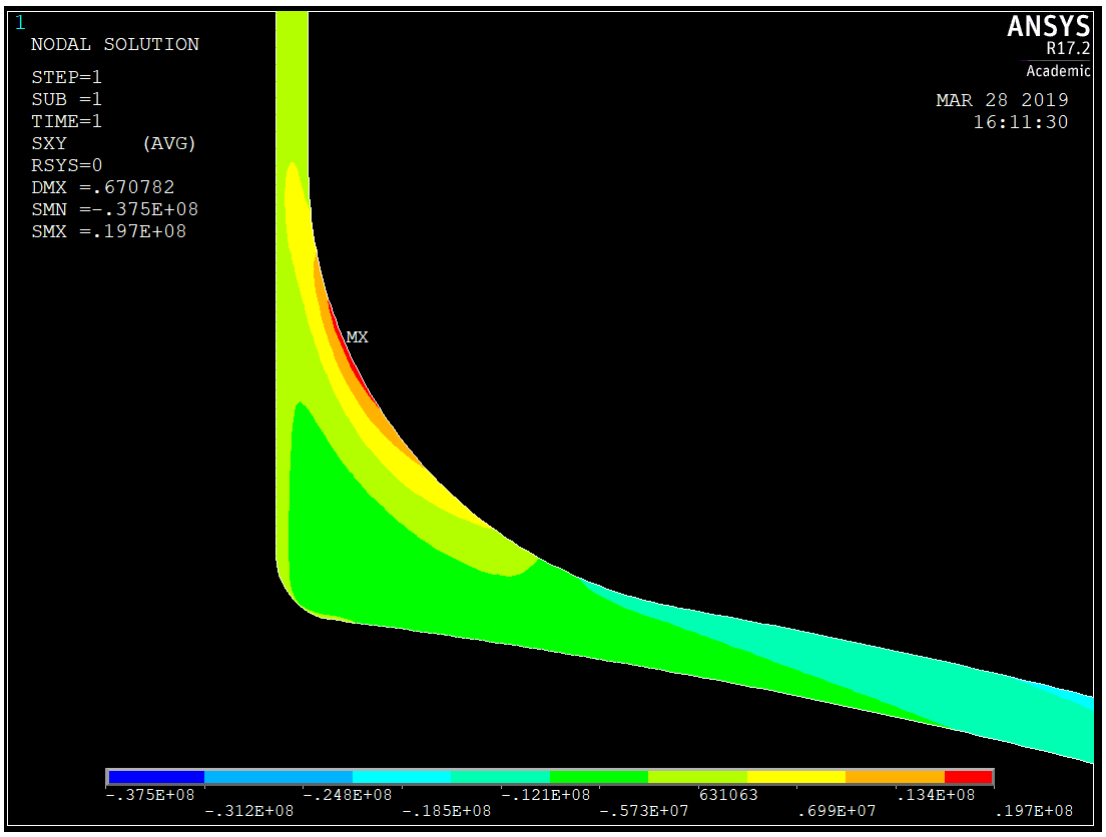

Figure 15: Shear Stress (RZ) Contour

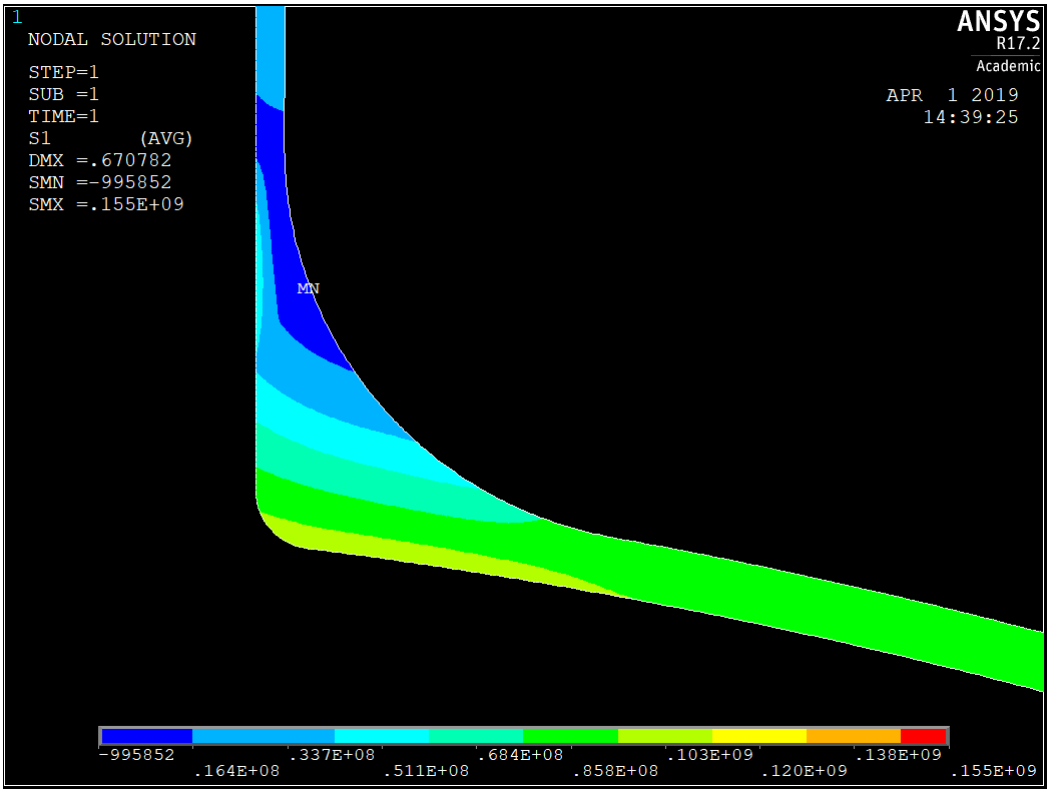

Figure 16: Principal Stress 1 (Circumferential)

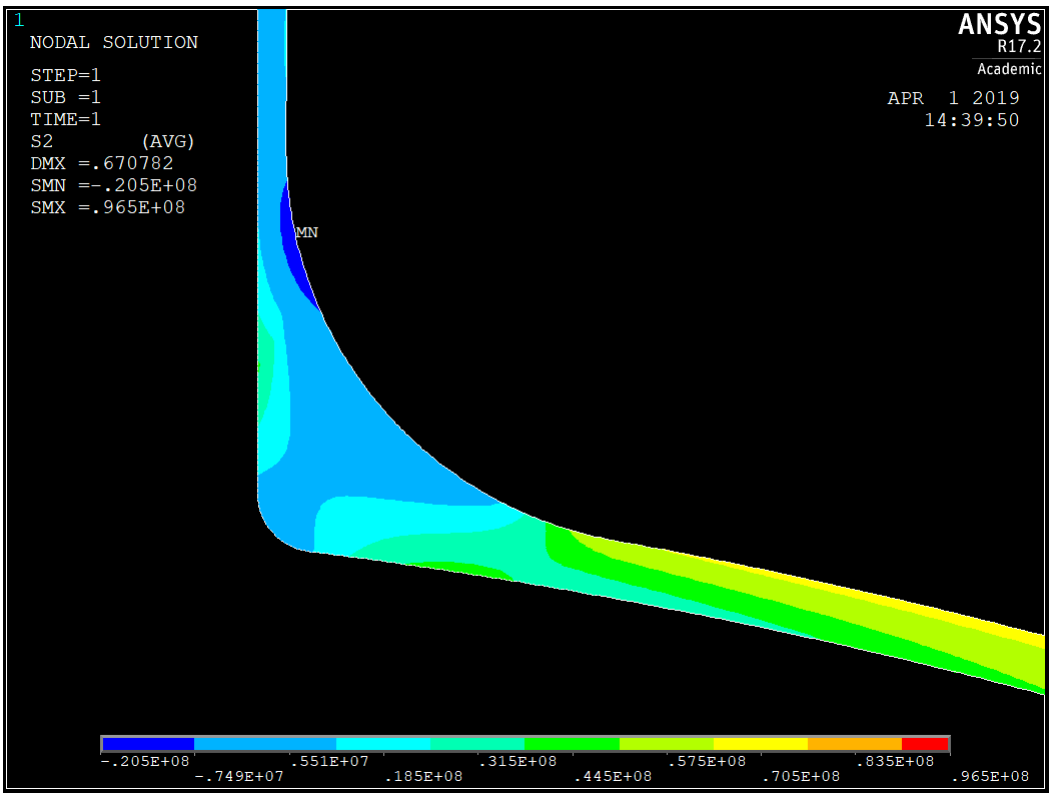

Figure 17: Principal Stress 2 (Radial/ ϕ)

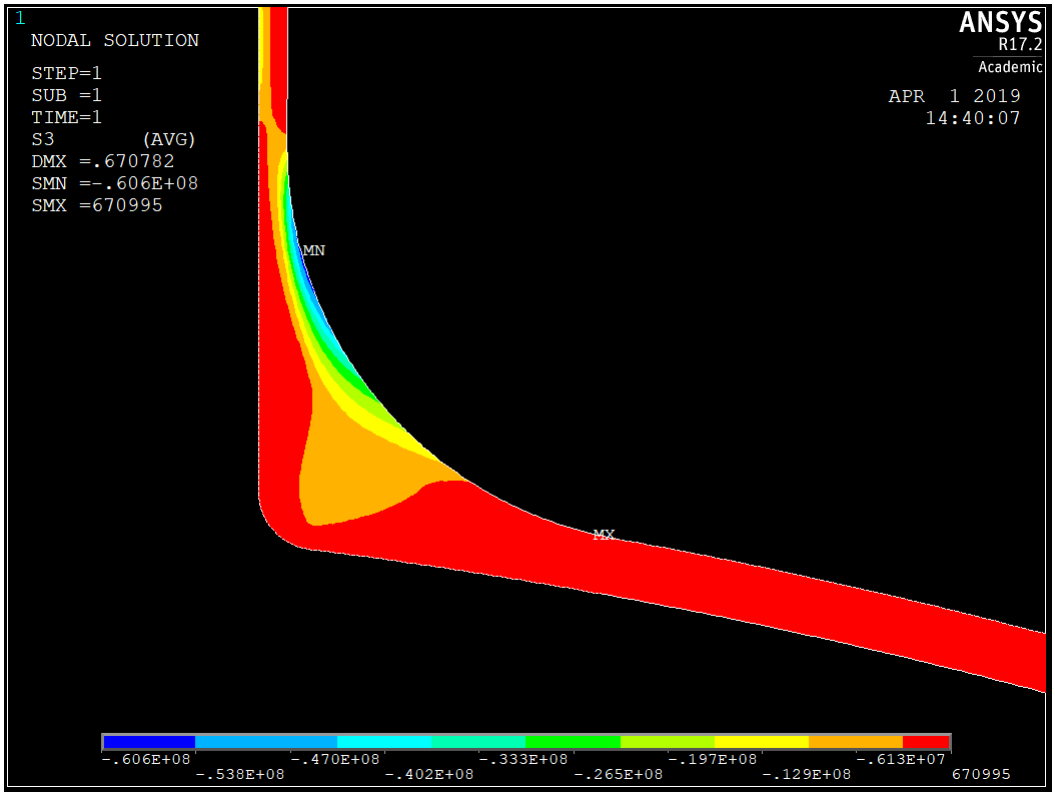

Figure 18: Principal Stress 3 (Axial in the cylindrical part, Radial in the hemispherical)

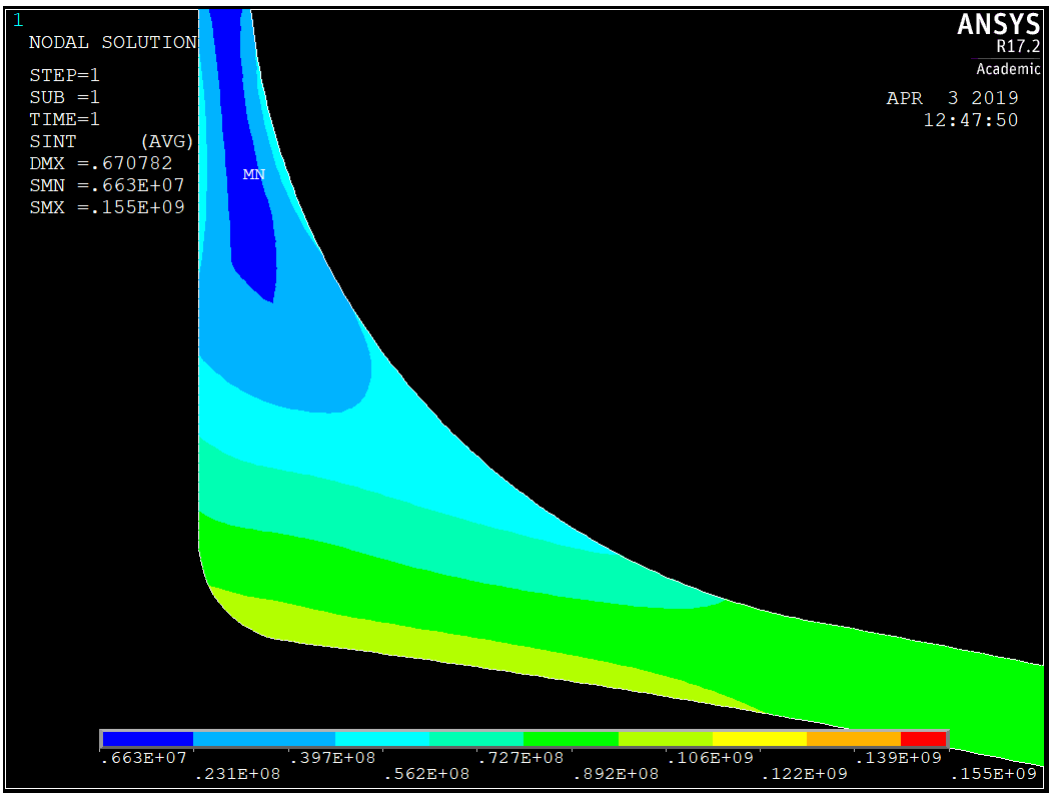

Figure 19: Von Mises Contour Plot

6 Conclusion

As the model was relatively simple, and computational time was considered during modelling decisions, the simulations were very quick to run. Following the convergence study and verification checks, the model can be considered to represent the operational considerations of the actual pressure vessel.

The comparisons to the analytic solutions were accurate with noticeable exceptions of those in the hemispherical section, so principal stresses were provided and those were found to be accurate. For graphical comparison a Von Mises contour plot was also included.

The shear stress was found to be greatest at the outer surface of the fillet between the nozzle and pressure vessel, while the von mises and circumferential stresses were found to be greatest at the inner surface of the join between the nozzle and pressure vessel.

References

[1] R J Roark. *Formulas for Stress and Strain*. McGraw-Hill, 4th edition, 1965.